



Published in final edited form as:

Nat Genet. 2015 August ; 47(8): 864–871. doi:10.1038/ng.3333.

## Relapsed neuroblastomas show frequent RAS-MAPK pathway mutations

Thomas F. Eleveld, M.Sci., Derek A. Oldridge, M.Sci., Virginie Bernard, Ph.D., Jan Koster, Ph.D., Leo Colmet Daage, M.Sci., Sharon J. Diskin, Ph.D., Linda Schild, B.Sc., Nadia Bessoltane Bentahar, M.Sci., Angela Bellini, Ph.D., Mathieu Chicard, M.Sci., Eve Lapouble, Ph.D., Valérie Combaret, PhD, Patricia Legoix-Né, M.Sci., Jean Michon, M.D., Trevor J. Pugh, Ph.D., Lori S. Hart, Ph.D., JulieAnn Rader, M.Sci., Edward F. Attiyeh, M.D., Jun S. Wei, Ph.D., Shile Zhang, M.Sci., Arlene Naranjo, Ph.D., Julie M. Gastier-Foster, Ph.D., Michael D. Hogarty, M.D., Shahab Asgharzadeh, M.D., Malcolm A. Smith, M.D., Ph.D., Jaime M. Guidry Auvil, Ph.D., Thomas B. K. Watkins, M.Sci., Danny A. Zwiijnenburg, B.Sc., Marli E. Ebus, B.Sc., Peter van Sluis, B.Sc., Anne Hakkert, M.Sci., Esther van Wezel, M.Sci., C. Ellen van der Schoot, M.D., PhD, Ellen M. Westerhout, Ph.D., Johannes H. Schulte, M.D., Ph.D., Godelieve A. Tytgat, M.D., Ph.D., M. Emmy M. Dolman, Ph.D., Isabelle Janoueix-Lerosey, Ph.D., Daniela S. Gerhard, Ph.D., Huib N. Caron, M.D., Ph.D., Olivier Delattre, M.D., Ph.D., Javed Khan, M.D., Rogier Versteeg, Ph.D., Gudrun Schleiermacher, M.D., Ph.D., Jan J. Molenaar, M.D., Ph.D., and John M. Maris, M.D.

Department of Oncogenomics, Academic Medical Center of the University of Amsterdam, the Netherlands (T.F.E., J.K., L.S., D.A.Z., M.E.E., P.S., A.H., E.M.W., E.M.D., R.V., J.J.M.); the Division of Oncology and Center for Childhood Cancer Research, Children's Hospital of Philadelphia (D.A.O., S.J.D., L.S.H., J.R., E.F.A., M.D.H., J.M.M.); the Perelman School of Medicine at the University of Pennsylvania (D.O., S.J.D., E.F.A., M.D.H., J.M.M.); the Children's Oncology Group Statistics and Data Center, University of Florida (A.N.); the U830 INSERM, RTOP Laboratory, ICGEX Platform and Département de Pédiatrie, Institut Curie, Paris, France (V.B., L.C.D., N.B., A.B., M.C., E.L., P.L.N., J.M., I.J.L., O.D., G.S.); Centre Léon Bérard, Lyon (V.C.); the University of Toronto (T.J.P.); the National Cancer Institute (J.S.W., S.Z., M.A.S., D.S.G., J.K.); the University of Florida (A.N.) and Nationwide Children's Hospital and Ohio State University College of Medicine (J.M.G-F.); The Children's Hospital of Los Angeles and The University of Southern California (S.A) the Department of Pediatric Oncology, Emma Children's Hospital, Academic Medical Center (G.A.T., H.N.C.); the Department of Experimental Immunohematology, Sanquin Research, Amsterdam and the Landsteiner Laboratory, Academic Medical Center (E.W., C.E.S.); Department of Pediatric Oncology and Hematology, Charité University Medicine, Berlin, German Consortium for Translational Cancer Research (DKTK), Heidelberg, Department of Pediatric Oncology and Hematology, University Children's Hospital Essen, Translational Neuro-Oncology, West German Cancer Center (WTZ), University Hospital

Mr Eleveld, Mr Oldridge and Dr Bernard and Drs Schleiermacher, Molenaar and Maris contributed equally to this work.

### Accession codes

The whole genome sequencing data have been deposited at the European Bioinformatics Institute under study accession number ID EGAS00001001184 for the French cases, and under accession number EGAS00001001183 for the Dutch cases. Sequence data for the US cases are available in dbGaP under accession phs000467. Whole exome sequencing data for neuroblastoma cell lines will be made available through the Sequence Read Archive (accession pending).

Essen, Essen, Germany (J.H.S.); the Translational Cancer Therapeutics Laboratory, Cancer Research UK London (T.B.K.W)

## Abstract

The majority of neuroblastoma patients have tumors that initially respond to chemotherapy, but a large proportion of patients will experience therapy-resistant relapses. The molecular basis of this aggressive phenotype is unknown. Whole genome sequencing of 23 paired diagnostic and relapsed neuroblastomas showed clonal evolution from the diagnostic tumor with a median of 29 somatic mutations unique to the relapse sample. Eighteen of the 23 relapse tumors (78%) showed mutations predicted to activate the RAS-MAPK signaling pathway. Seven events were detected only in the relapse tumor while the others showed clonal enrichment. In neuroblastoma cell lines we also detected a high frequency of activating mutations in the RAS-MAPK pathway (11/18, 61%) and these lesions predicted for sensitivity to MEK inhibition *in vitro* and *in vivo*. Our findings provide the rationale for genetic characterization of relapse neuroblastoma and show that RAS-MAPK pathway mutations may function as a biomarker for new therapeutic approaches to refractory disease.

## Introduction

Neuroblastoma is a pediatric tumor of the peripheral sympathetic nervous system. Tumor behavior varies from spontaneous regression to incurable progression. Patients with high-risk neuroblastoma have a survival rate of less than 50%<sup>1, 2</sup>, despite extensive treatment involving chemotherapy, surgery, radiation therapy and immunotherapy. In a majority of patients an initial response is observed, however, up to 60% of these patients subsequently relapse with therapy resistant tumors<sup>3-5</sup>. Genetic alterations including *MYCN* amplification and segmental chromosome alterations such as 1p deletion, 11q deletion or 17q gain are associated with poor prognosis<sup>6-9</sup>; however, it is unknown which genetic defects are associated with disease relapse.

To date, 389 primary neuroblastoma DNAs obtained at the time of diagnosis have been profiled by Next Generation Sequencing (NGS) techniques<sup>10-13</sup>. These studies documented a relative paucity of somatic mutations, with activating mutations in *ALK* and inactivating mutations in *ATRX* being most frequent, but each in less than 10% of cases studied. These studies challenge the notion of precision medicine based on somatic genetic alterations in primary neuroblastoma tumors alone. Importantly, none of these large-scale studies considered the tumor genome at relapse, partly because patients are rarely subjected to a tumor biopsy at the time of disease progression since current diagnostic radiology techniques such as meta-iodobenzylguanidine scintigraphy are highly sensitive and specific<sup>14</sup>.

Recently, sequencing of the *ALK* locus in neuroblastomas at the time of relapse identified 14 activating mutations in 54 cases (26%)<sup>15</sup>, suggesting that the frequency of *ALK* aberrations is higher in relapsed neuroblastoma genomes. This implies selection of tumor cells with alterations in genes that mediate neuroblastoma relapse. Therefore, to identify genetic

alterations associated with relapsed neuroblastoma, we performed whole genome sequencing of 23 triplets of primary tumor, relapsed tumor and constitutional DNA.

## Results

### Clonal evolution

We sequenced the genomes of 23 triplets of lymphocyte, primary tumor and relapse neuroblastoma (Supplementary Table 1). Tumors were of all stages and with variable outcome, with the only eligibility criteria being the availability of high-quality DNA from the triplet samples. There was a roughly equal distribution of cases between low-, intermediate- and high-risk groups<sup>5</sup>. The median time from diagnosis to relapse was 11.3 months (range 1–90). Twenty-one of the 23 subjects in this study received chemotherapy prior to relapse, and eight also received radiation therapy, according to internationally accepted treatment protocols (Table 1). This means that all patients received similar chemotherapy regimens, with high-risk patients additionally receiving radiation therapy and high-dose chemotherapy with stem cell rescue. No patient on this study received targeted inhibitors to any oncogenic pathway between the time of diagnosis and relapse. The majority of low-risk cases received chemotherapy due to site and/or size of the primary tumor.

Sequence data were analyzed for somatic mutations resulting in amino acid changes or located within splice site regions within 3 bp of an exon, as well as for focal structural aberrations of regions containing five genes or less (Supplementary Table 2,3 and 4). There was a median of 14 more mutations in the relapsed samples compared to the samples at diagnosis (Figure 1 and Supplementary Figure 1). On average, 28% of the mutations detected in the primary tumor were also detected at relapse, showing that primary and relapsed tumors were of common descent. To gain more insight into the clonal architecture, we estimated the cancer cell fraction (CCF) of all somatic mutations using a customized reimplementation of a previously described Bayesian approach<sup>16</sup>, which infers CCF from mutant allele fractions determined by sequencing and accounts for contamination and locus-specific copy number. This analysis yielded a median CCF of 61% for mutations detected in the primary but lost in the relapse tumor, compared to a median CCF of 90% for primary tumor mutations shared with the relapse (Supplementary Figure 2A), a pattern that is consistent with subclonal outgrowth of the relapsed tumor. Furthermore, we estimated a median CCF of 83% for all relapse tumor mutations compared to a median CCF of 75% for all primary tumor mutations, indicating clonal enrichment of a subset of mutations at relapse (Supplementary Figure 2B). Comparison of genes affected by smaller structural events and chromosomal copy number alterations of primary and paired relapse tumors showed similar results with a subset of aberrations being shared, but many being detected only in the primary or relapse tumor (Figures 1C, 1D, Supplementary Figure 3 and Supplementary Table 4).

### Enrichment of mutations predicted to activate the RAS-MAPK signalling pathway

Unbiased pathway analysis<sup>17</sup> using WGS data from the relapse samples on a per patient basis identified a strong enrichment ( $p=6.1 \times 10^{-7}$ ) for mutations in genes associated with

RAS-MAPK signaling (Supplementary Table 5). We next filtered the identified genes against the Cancer Gene Census<sup>18</sup> and subsequently focused on hotspot regions by selecting COSMIC annotated mutations, to identify events that are well annotated to activate this pathway. Fifteen out of 23 relapse samples contained somatic mutations that meet these criteria. In addition, three relapse samples showed structural alterations involving these RAS-MAPK pathway genes, so aberrations in this pathway were detected in 18/23 relapse samples (78%) and all were consistent with pathway activation (Table 2). Eleven RAS-MAPK activating mutations that were present in primary tumors were all preserved in the corresponding relapses. Seven mutations were not detectable in the primary tumor at the sequencing depth achieved and therefore ultra-deep sequencing was employed to determine if these mutations were present in fractions under the WGS detection limit. The *ALK* mutation in N607 was found in the primary tumor, while the other mutations were undetectable (Supplementary Figure 4A). Structural aberrations were assayed using PCR based methods. Only the *ALK* rearrangement in N790 was shown to be present at low frequency in the primary tumor (Supplementary Figure 4B).

*ALK* aberrations occurred in 10 relapse tumors and were also detected by WGS in 7 of the corresponding primary tumors. All detected SNVs have been proven to constitutively activate this receptor tyrosine kinase known to activate RAS-MAPK signaling<sup>19</sup>. Furthermore, one relapse showed a *de novo* amplification giving rise to a *PPM1G-ALK* fusion gene, that activates the RAS-MAPK pathway when expressed in neuroblastoma cell lines (Supplementary Figure 5).

Two tumors showed relapse specific inactivation of the *NFI* tumor suppressor gene, either through homozygous deletion or heterozygous deletion combined with a splice site mutation (Supplementary Figure 6). *NFI* inactivation has been reported in neuroblastoma and confers activation of RAS-MAPK signaling and resistance to retinoic acid<sup>20</sup>. One pair of primary and relapse tumors showed a heterozygous mutation in *PTPN11*. Mutations in *PTPN11* activate RAS-MAPK signaling and the identified A72T mutation has been reported in leukemia and neuroblastoma<sup>12, 21</sup>.

One relapse tumor showed a tandem duplication in the *BRAF* gene that was not detected in the primary tumor. This rearrangement leads to expression of a *BRAF* transcript that encodes an elongated protein with two kinase domains. Expression of this tandem duplication in the *BRAF* gene in a neuroblastoma cell line induced activation of the RAS-MAPK pathway (Supplementary Figure 7). Taken together, the somatic mutations detected in this case series shown to activate the RAS-MAPK pathway were mutually exclusive, with no case showing two somatic events known to hyperactivate this growth promoting pathway.

We hypothesized that RAS-MAPK activating mutations exhibit relapse-specific enrichment due to treatment. We therefore performed a clonality analysis, comparing CCF estimates for RAS-MAPK mutations between paired primary (CCF<sub>p</sub>) and relapse (CCF<sub>r</sub>) tumors (Figure 2 and Supplementary Figure 8). RAS-MAPK mutations were almost universally present within major subclonal populations at relapse, as indicated by CCF<sub>r</sub> > 0.5 with probability >90% under the posterior distribution for 14 out of 15 relapse tumors. In 7 out of 15 tumor pairs there was strong evidence of relapse-specific enrichment of RAS-MAPK mutations—

including mutations in *ALK* (4 pairs), *HRAS* (1 pair), *KRAS* (1 pair), and *NF1* (1 pair)—based on a criterion of  $CCF_r > CCF_p$  with probability >90% for each pair. By contrast, the probability that  $CCF_r > CCF_p$  fell within 20–80% bounds for the remaining 8 pairs, indicating that RAS-MAPK mutations that were already present in the primary tumor are retained at relapse. Collectively, these results support RAS-MAPK mutations as somatic drivers that undergo positive selection over the course of neuroblastoma treatment.

### Chromosomal aberrations

Three relapse samples showed homozygous deletions in the *CDKN2A* locus, encoding the tumor suppressor proteins p14ARF and p16, while both alleles of *CDKN2A* were present in the corresponding primary tumors (Supplementary Figure 9). *CDKN2A* deletions were previously reported as frequent events in neuroblastoma relapses<sup>22</sup>. Other relapse-specific segmental chromosome defects were detected, including loss of 6q (5 cases) and loss of 17p (3 cases). Furthermore, we detected relapse specific aberrations that are frequently detected in primary neuroblastoma and are associated with poor prognosis, including loss of chromosome 1p (1 case) and 11q (3 cases; Figure 1C and Supplementary Figure 3)<sup>7,9</sup>.

### RAS-MAPK pathway mutations render neuroblastoma cell lines susceptible to MEK inhibition

To determine if neuroblastoma cell lines contain RAS-MAPK mutations, we analyzed whole genome sequencing data of a series of human-derived neuroblastoma cell lines for mutations in *ALK*, *NRAS*, *HRAS*, *KRAS*, *BRAF*, *PTPN11* and *NF1*. Eleven of the 18 cell lines showed such mutations (Supplementary Table 6 and Supplementary Figure 10).

We tested our cell line panel for sensitivity to the MEK inhibitors Trametinib, Cobimetinib and Binimetinib, to determine the relationship between mutation status and drug sensitivity. The data show a clustering into four groups with increasing sensitivity to MEK inhibition: cell lines i) without RAS-MAPK mutations; ii) with *ALK* mutations; iii) with *NF1* mutations; and iv) with *RAS/BRAF* mutations (Supplementary Figure 11). In the *RAS/RAF* mutated lines MEK inhibitor treatment causes near complete cell cycle arrest at low nM concentrations, while in the *NF1* and *ALK* mutated lines the effect on cell cycle inhibition is less robust (data not shown). When expressed as concentrations at which cell growth was inhibited by 50% (GI50), there were significant differences in sensitivity between cell lines with and without RAS-MAPK mutations (Figure 3A–C). The GI50 values were highly correlated in the cell line panel (Supplementary Figure 12) suggesting an on-target effect ( $r^2=0.49–0.79$ ,  $p<0.01$ ). The relationship between mutation status and sensitivity to MEK inhibition was also observed in an independent published dataset<sup>23</sup> (Supplementary Figure 13).

To validate that *ALK* and *RAS* mutations directly activate the RAS/MAPK pathway in neuroblastoma cells, we inducibly expressed an *ALK F1174L* and an *NRAS v61Q* mutation in two cell lines that did not harbor RAS-MAPK mutations. Expression of both mutated proteins causes activation of this pathway (Supplementary Figure 14). We have shown previously that knockdown of *NF1* causes hyperactivated RAS-MAPK signaling in neuroblastoma cell lines<sup>20</sup>.

We next treated various human neuroblastoma-derived cell line xenograft models, representing the four groups mentioned above, with the MEK inhibitor Binimetinib. SK-N-AS xenografts, which harbor an *NRAS* p.Q61K mutation, showed inhibition of tumor growth and increased survival when treated with Binimetinib in a dose dependent fashion (Figure 3D). NBL-S xenografts have an inactivating mutation in one allele of *NF1*, and a near absence of NF1 protein expression (Supplementary Figure 15), and also showed inhibition of growth. Conversely, treatment of Kelly and IMR-5 xenografts showed no effect on tumor growth. IMR-5 does not have RAS-MAPK pathway mutations detectable by whole exome sequencing (data not shown), while Kelly harbors an *ALK F1174L* mutation.

We then determined if inhibition of cell growth corresponds with inhibition of the RAS-MAPK pathway in the cell lines that were used for the murine xenograft experiments. Cell lines were treated with increasing concentrations of Binimetinib *in vitro* for 24 hours and screened for ERK phosphorylation (Supplementary Figure 16). The three lines with RAS-MAPK mutations show phosphorylation of ERK in untreated conditions, reaffirming that these mutations indeed lead to activation of this pathway. Upon exposure to Binimetinib, SK-N-AS and NBL-S showed a dose dependent decrease in phosphorylated ERK (pERK), while Kelly showed no significant change. These data suggest that the minimal effect of MEK inhibition *in vitro* and absence of effect *in vivo* for the Kelly cell line may be due, at least in part, continued ERK phosphorylation. To confirm that the response we observed *in vivo* is also due to target inhibition we analyzed ERK phosphorylation in the xenografts that responded to treatment, and demonstrated a dose dependent decrease in pERK (Supplementary Figure 17).

## Discussion

Recent studies utilizing NGS methodologies indicate firstly a low mutation rate in primary neuroblastoma tumors, with a mean of 15 nonsynonymous mutations per sample, and secondly a paucity in recurrently affected genes<sup>10–13</sup>. Since relapsed high-risk neuroblastoma tumors often demonstrate significant chemotherapy resistance and are typically lethal, we hypothesized that mutational spectrum of relapsed disease would be different than the primary tumors, and may mediate therapy resistance.

In this study we characterized the genomes of 23 relapsed neuroblastomas and compared each to the genome of the corresponding primary tumor. We show that the relapsed tumors generally contain more mutations and structural aberrations, and that clonal selection takes place between the primary tumor and the relapse. We found that 18/23 relapse tumors harbored mutations predicted to hyperactivate the RAS-MAPK signaling pathway, and that cell lines containing similar mutations show sensitivity to MEK inhibition, a downstream node in the canonical growth-promoting pathway. These results provide a strong rationale for recommending a biopsy and genomic characterization of relapsed neuroblastoma tumors and for prioritizing clinical testing of MEK inhibition strategies in the treatment of relapsed neuroblastoma.

Due to the sensitivity and specificity of modern imaging modalities, the diagnosis of neuroblastoma relapse rarely requires a tumor biopsy. In addition, until recently there has

been no realistic potential for therapeutic benefit based on biopsy results, and therefore very few relapse neuroblastoma samples are available for study. Here we collected high quality material from 23 relapse-tumor pairs across the spectrum of neuroblastoma phenotypes including those assigned to high-, intermediate-, and low-risk groups<sup>5</sup>. The only inclusion criterion for this study was the availability of matched samples, but some cases may have been biopsied due to an unusual clinical course. Indeed there is a fairly high number of intermediate and low risk tumors which normally do not show frequent relapses<sup>5</sup>. However, the frequency of RAS-MAPK mutations did not differ between groups, so it is unlikely that the overrepresentation analysis is influenced by this bias.

The high frequency of RAS-MAPK pathway mutations at diagnosis in this cohort was unexpected, since such high frequencies were not reported in WGS series of primary tumors<sup>10–13</sup>. It is possible that the presence of these lesions in a diagnostic sample is a biomarker of a more aggressive clinical course and higher likelihood of relapse. These findings need to be validated in a prospective patient cohort.

We detected several recurrent structural aberrations at the time of relapse. Partial loss of chromosome 6q was observed in 5 relapses and homozygous deletion of *CDKN2A* in 3 relapses. Both events are infrequent in primary neuroblastoma and present interesting targets for further research. Furthermore, neuroblastoma associated aberrations like loss of 1p and 11q were observed in the relapse and not in the primary tumor, indicating that these events might not be tumor initiating but rather are crucial steps in neuroblastoma tumor evolution<sup>24</sup>.

Events affecting RAS-MAPK signaling were detected in 18/23 relapse samples. In 4 cases we identified structural variants, highlighting the benefit of WGS for detecting the full spectrum of genetic alterations. In 7/18 cases these mutations were observed only in the relapse tumor, which indicates that analysis on primary tumor samples is not sufficient to guide the choice of treatment for neuroblastoma relapses. These findings are in line with the *de novo* occurrence of *ALK* mutations reported previously<sup>15</sup>.

The observation that several RAS-MAPK mutations were found in the relapse but not in the corresponding primary tumors, favors a model where subclones with secondary driver mutations expand over time, possibly under the selective pressure of chemotherapy, as was recently described for chronic lymphocytic leukemia<sup>25</sup>. Whether these mutations occurred between the primary and the relapse tumor, were present in levels below detection limits, or were undetectable due to spatial heterogeneity of the primary tumor remains to be determined.

It has been firmly established that mutations in the RAS-MAPK pathway can occur as resistance mechanisms against targeted kinase inhibitors<sup>26</sup>, however, no targeted inhibitors were used in the treatment of our patient cohort. Mutations in the RAS-MAPK pathway may also be associated with resistance to conventional cytotoxic therapies in neuroblastoma, but more research is needed to establish the molecular basis behind this.

The *ALK* gene was mutated in 10 relapse samples and it is known that the most frequent *ALK* mutations in neuroblastoma activate the RAS-MAPK signaling pathway<sup>27</sup>. The results

of our xenograft therapeutic studies indicate that single agent treatment with a MEK inhibitor might not be effective in *ALK* mutated tumors. However, the observation that *in vitro* the *ALK* mutated cell lines consistently showed some sensitivity to MEK inhibition suggests that activated RAS-MAPK does play a role in *ALK* mutated neuroblastoma and warrants further investigation on the use of MEK inhibitors in combination therapies. *ALK* inhibitors have proven to be effective in the treatment of *ALK* mutated tumors<sup>28</sup>, but some mutations are associated with resistance to currently available *ALK* inhibitors<sup>19</sup>. Therefore combined MEK and *ALK* inhibition may improve response in tumors containing such mutations. Combination with targeted inhibitors against other pathways that are activated in *ALK* mutated neuroblastoma, such as PI3K and mTOR<sup>29, 30</sup>, may also improve therapeutic efficacy.

We also detect mutations in *NF1*, *BRAF*, *PTPN11*, *FGFR1* and the three *RAS* genes, and all lesions in the RAS-MAPK pathway were mutually exclusive. Cell lines with RAS-MAPK mutations show moderate to high sensitivity to MEK inhibitors, and treatment with the inhibitor Binimetinib of SK-N-AS xenografts, which contain an *NRAS* mutation, as well as NBL-S, which has a loss of *NF1*, results in a significant therapeutic efficacy. This suggests that MEK inhibition may have clinical benefit in treatment of neuroblastoma relapses containing RAS-MAPK mutations.

Our study provides strong rationale for performing biopsies and genomic characterization of relapsed neuroblastomas, with the prospect of direct patient benefit. We show that RAS-MAPK pathway mutations occur frequently in relapsed neuroblastoma, and propose matching such pathway lesions to novel therapies such as MEK inhibition. A prospective clinical trial consisting of biopsy and NGS-based selection of targeted therapy will be required to determine the clinical implication of this newly defined genetic landscape of relapsed neuroblastoma.

## Methods

### Sample collection/patient selection

Inclusion criteria for this study were histopathologic confirmation of neuroblastoma at original diagnosis and the presence of biopsy material from a subsequent relapse specimen. Patients were included in this study following informed consent from the parents or guardians, with oversight from the respective human subjects review boards. Somatic *ALK* mutation status has been reported for samples FR\_NB0175, FR\_NB308, FR\_NB399, FR\_NB1224, FR\_NB1269 and FR\_NB13821<sup>24</sup>.

### Whole Genome Sequencing- summary

Whole genome sequencing was performed by Complete Genomics, Inc. (CGI) to an average coverage of 50X per sample (for Dutch and American patient material and cell line material)<sup>31</sup>, or using Illumina HighSeq2500 instruments to an average coverage of 80x per sample (for French patient material). Material from one patient (lymphocytes/primary/relapse) was in all cases sequenced on the same platform. See Supplementary Table 1 for details on sequencing results. Estimation of normal tissue contamination and whole genome

segmentation was performed on all primary/normal and relapse/normal pairs with Sequenza software v2.1.0 using both binned coverage ratio data and SNV allelic ratios as input<sup>32</sup>. Coverage based copy number plots were generated as previously described<sup>11</sup>, with the exception that values were corrected for ploidy and purity as determined by Sequenza. The R2 bioinformatics platform (<http://r2.amc.nl>) and Circos<sup>33</sup> were used for analysis and visualization.

## WGS – Complete Genomics

Potential somatic variants were determined with the CallDiff algorithm with somatic output as available in the CGAtools v1.3.0 package, maintained by Complete Genomics Inc. Every tumor was compared to its matched blood sample across the genome. The somatic output files were then filtered to those regions where coding sequences are defined within the UCSC refflat. Subsequently silent mutations were removed from the analysis. In addition, we determined the presence of somatic splice-site variants in the three bases surrounding exons as defined by the UCSC refflat data. Variants with a somatic score > 0.05 (for NL\_041, NL\_571 and NL\_N607) or Somatic Quality high (rest of patients) were included in the analysis.

For structural variants comparisons between tumor and lymphocyte genomes were performed with the JunctionDiff and Junction2Event algorithm from CGAtools. These somatic events were filtered with the following criteria: events annotated as artefacts, footprints smaller than 70 bases, less than 10 discordant mate pairs, under-represented repeats, and presence in a set of baseline genomes (as provided on the website of Complete Genomics (B36baseline-junctions.tsv)). Of the remaining entries, we kept the following events:

- I.** Exon\_bites where both ends of a junction are within the same gene, and in addition affect an exonic sequence,
- II.** Breaks by inversion, where both ends of a junction land within a gene, thereby damaging both genes, but leaving the genes in between unaffected.
- III.** Potential fusion genes which are strand-matched, where both ends of a junction land within a gene, and the resulting end product fits in terms of orientation of both genes.
- IV.** Regions (deletions/(tandem) duplications) of up to 1 megabase, containing up to five genes.

## WGS - Illumina

Whole genome sequencing was performed using a Illumina Hi-seq2500, with 90bp paired-ends reads for 6 tumors and 100 bp paired-end reads for the remaining two. Following alignment with Hg19 using BWA<sup>34</sup>, bam files were cleaned up according to the Genome Analysis Toolkit (GATK) recommendations<sup>35</sup>.

Variant calling was performed in parallel using 3 variant callers: GenomeAnalysisTK-2.2-16, Samtools-0.1.18 and MuTect-1.1.430<sup>34-36</sup>,. Annovar-v2012-10-23<sup>37</sup> with cosmic-v64 and dbsnp-v137 were used for annotation. Single nucleotide variants (SNVs) with a quality

under 30, a depth of coverage under 6 or with less than 2 reads supporting the variant were filtered out, as were variants reported in more than 1% of the population in the 1000 genomes<sup>38</sup> or Exome Sequencing Project (Exome Variant Server, NHLBI GO Exome Sequencing Project (ESP), Seattle, WA (URL: <http://evs.gs.washington.edu/EVS>)).

Variants were then filtered to those regions where coding sequences are defined, or to variants in the three bases surrounding exons. Subsequently silent mutations were removed from the analysis. Tumor and corresponding constitutional genomes were compared using the SAMtools Mpileup algorithm<sup>34</sup> and non-somatic variants were discarded from the analysis.

Structural variants (SVs) including deletions, inversions, tandem duplications and translocations were analyzed using DELLY-v0.5.5 with standard parameters<sup>39</sup>. In tumors, at least 10 supporting reads were required to make a call and 5 supporting reads for the sample NB0175 with a coverage of only 40X. To predict SVs in constitutional samples for subsequent somatic filtering, only 2 supporting reads were required. To identify somatic events, all the SVs in each normal sample were first flanked by 500 bp in both directions and any SV called in a tumor sample which was in the combined flanked regions of respective normal sample was removed. Deletions with more than 5 genes impacted or larger than 1Mb and inversions or tandem duplications covering more than 4 genes were removed. We focused on exonic and splicing events for deletions, inversions, and tandem duplications. For translocations, we kept all SVs that occurred in intronic, exonic, 5'UTR, upstream or splicing regions.

### Clonality analysis

Estimation of the cancer cell frequency of somatic mutations was performed using the Bayesian method of Carter et al. to infer posterior intervals without clustering for comparison<sup>25, 40</sup>. Namely, we assumed that the expected allele fraction of a mutation in a sample of tumor purity “ $\alpha$ ”, total somatic copy number “ $q$ ”, and mutation multiplicity “ $s$ ” can be expressed as a function of the cancer cell fraction “ $c$ ”:  $f(c) = \alpha c s / (2 (1 - \alpha) + \alpha q)$ . Given a uniform prior on “ $c$ ”, the posterior density of “ $c$ ” is therefore proportional to  $\text{Binom}(a | N, f(c))$ , where “ $a$ ” is the variant read count and “ $N$ ” is the total read count. While “ $\alpha$ ” and “ $q$ ” are estimated by Sequenza, the mutation multiplicity “ $s$ ” is generally not known. However, under the parsimony assumption that a mutation occurs only once within a tumor’s evolutionary history, we can bound “ $s$ ” by  $1 \leq s \leq m \leq q$ , where “ $m$ ” is the major allelic copy number of the mutation locus, which is estimated by Sequenza. We therefore modeled the posterior distribution under two assumptions:  $s = 1$  (biased toward higher clonality estimates) as well as  $s = m$  (biased toward lower clonality estimates).

Estimation of CCF was also performed using PyClone v0.12.7 as an alternative method for comparison<sup>41</sup>. For each primary or relapse tumor, PyClone was run on all somatic coding point mutations using the “parental\_copy\_number” method and “pyclone\_beta\_binomial” density, with estimates of tumor purity and allelic copy number from Sequenza provided as necessary inputs. The Markov Chain Monte Carlo (MCMC) step of PyClone was run for 10,000 iterations with burn-in and thin parameters set to 1,000 and 10, respectively,

resulting in 900 independent samples from the posterior distribution of cancer cell fraction per mutation. Otherwise, default options for PyClone were used.

### CancerMutationAnalysis

To identify pathways or processes that were frequently affected in neuroblastoma relapse tumors we used the CancerMutationAnalysis R package<sup>17</sup>. Somatic mutations detected only in the relapse and detected in the relapse and primary for all tumors were used as input. This algorithm is not suitable for the analysis of structural variants, so these were not included in this analysis. P-values were generated using the “permutation null method without heterogeneity” and signify enrichment of mutated genes associated with a certain GO Biological Process category across all relapse tumors.

### Cell lines

All cell lines were cultured in Dulbecco’s Modified Eagle’s Medium (DMEM) or RPMI-1640 supplemented with 10% FBS, 20 mmol/L L-glutamine, 10 U/mL penicillin, and 10 µg/mL streptomycin and maintained at 37°C under 5% CO<sub>2</sub>. Cell line identities are regularly confirmed by short tandem repeat profiling using the PowerPlex16 system and GeneMapper software (Promega).

### Cell viability assays in response to MEK inhibition

For cell viability assays, 2.5–25 × 10<sup>3</sup> cells were seeded in 50 µL in 96 well plates 1 day before treatment with one of three MEK inhibitors. Binimetinib, Trametinib, or Cobimetinib (Selleckchem) was added in 7-point fivefold dilution series and cell viability was assayed by MTT (Sigma) after 72hrs as described previously<sup>42</sup>. All experiments were performed in triplicate and values were compared to solvent treated controls.

GI50 values were determined by calculating  $100 \times (T - T_0)/(C - T_0)$  for every drug concentration, where T = optical density for a certain drug concentration at T=72h, T<sub>0</sub> = optical density at T=0 (before adding drug), C = optical density of solvent treated controls at T=72h. Curves were fitted on the data points using non-linear regression in Graphpad5 (log(inhibitor) vs. response -- Variable slope) and GI50 values were interpolated from these curves. If curves did not reach 50% growth inhibition the GI50 value was set at 10µM.

### Whole exome sequencing of neuroblastoma cell lines

Whole exome sequencing of neuroblastoma cell lines SK-N-AS, NBL-S, Kelly and IMR-5 was performed using in-solution hybrid capture<sup>43</sup> followed by Illumina sequencing, as described previously<sup>12</sup>. A

### MEK inhibition in murine xenotransplants

The human neuroblastoma-derived cell lines SK-N-AS, NBL-S, Kelly and IMR-5 were xenotransplanted subcutaneously in CB17 SCID<sup>-/-</sup> mice. Once the engrafted tumors reached 200 mm<sup>3</sup>, animals were to oral treatment with Binimetinib (Novartis) at 3 mg/kg (n=10), 30 mg/kg (n=10) or vehicle only (n=10) by simple randomization. Mice were treated twice daily and tumor size was monitored three times weekly, and all investigators other than the mouse technician were blinded to group allocation and study outcomes until all

mice completed a trial. Tumor burden was determined according to the formula  $(\pi/6) d^2$ , where  $d$  represents the mean tumor diameter obtained by caliper measurement. Statistical analysis was performed using a two-tailed  $t$  test at each time point with  $p$ -values  $< 0.05$  indicating significance (\*) between vehicle and each of the treatment groups. All studies were performed in accordance with the Children's Hospital of Philadelphia Institutional Animal Care and Use Committee and animals were euthanized as soon as tumor volume exceeded  $3 \text{ cm}^3$ .

## Supplementary Material

Refer to Web version on PubMed Central for supplementary material.

## Acknowledgments

Supported in part by US National Institutes of Health grants RC1MD004418 to the TARGET consortium, and CA98543 and CA98413 to the Children's Oncology Group and supported in part by a Grant throughout the University of Pennsylvania Genome Frontiers Institute. In addition, this project was funded in part with Federal funds from the National Cancer Institute, National Institutes of Health, under Contract No. HHSN261200800001E. The content of this publication does not necessarily reflect the views of policies of the Department of Health and Human Services, nor does mention of trade names, commercial products, or organizations imply endorsement by the U.S. Government. The Binimetinib xenograft studies were supported through a research collaborative agreement between the Children's Hospital of Philadelphia and Novartis Pharmaceuticals. In France, this study was supported by the "Annenberg Foundation" and the "Nelia and Amadeo Barletta Foundation". Funding was also obtained from SiRIC/INCa (Grant INCa-DGOS-4654) and from the CEST of Institut Curie. This study was also funded by the Associations Enfants et Santé, Association Hubert Gouin Enfance et Cancer, Les Bagouz à Manon, Les amis de Claire. Deep sequencing experiments were conducted on the Institut Curie's ICGex NGS platform funded by the EQUIPEX "investissements d'avenir" program (ANR-10-EQPX-03) and ANR10-INBS-09-08 from the Agence Nationale de la Recherche, and by the Cancropôle Ile-de-France. In the Netherlands this study was supported by grants from the Villa Joep Foundation, KIKa and the Netherlands Cancer Foundation. The authors would like to thank Nicole Ross for sample preparation and quality control.

## Reference List

1. Hero B, et al. Localized Infant Neuroblastomas Often Show Spontaneous Regression: Results of the Prospective Trials NB95-S and NB97. *Journal of Clinical Oncology*. 2008; 26:1504–1510. [PubMed: 18349403]
2. Park JR, et al. Children's Oncology Group's 2013 blueprint for research: Neuroblastoma. *Pediatr Blood Cancer*. 2013; 60:985–993. [PubMed: 23255319]
3. Simon T, et al. Treatment and outcomes of patients with relapsed, high-risk neuroblastoma: Results of German trials. *Pediatr Blood Cancer*. 2011; 56:578–583. [PubMed: 21298742]
4. Maris JM. Recent advances in neuroblastoma. *N Engl J Med*. 2010; 362:2202–2211. [PubMed: 20558371]
5. Cohn SL, et al. The International Neuroblastoma Risk Group (INRG) Classification System: An INRG Task Force Report. *Journal of Clinical Oncology*. 2009; 27:289–297. [PubMed: 19047291]
6. Bown N, et al. Gain of Chromosome Arm 17q and Adverse Outcome in Patients with Neuroblastoma. *N Engl J Med*. 1999; 340:1954–1961. [PubMed: 10379019]
7. Attiyeh EF, et al. Chromosome 1p and 11q Deletions and Outcome in Neuroblastoma. *N Engl J Med*. 2005; 353:2243–2253. [PubMed: 16306521]
8. Seeger RC, et al. Association of Multiple Copies of the N-myc Oncogene with Rapid Progression of Neuroblastomas. *N Engl J Med*. 1985; 313:1111–1116. [PubMed: 4047115]
9. Caron H, et al. Allelic Loss of Chromosome 1p as a Predictor of Unfavorable Outcome in Patients with Neuroblastoma. *N Engl J Med*. 1996; 334:225–230. [PubMed: 8531999]
10. Cheung NK, et al. Association of age at diagnosis and genetic mutations in patients with neuroblastoma. *JAMA*. 2012; 307:1062–1071. [PubMed: 22416102]

11. Molenaar JJ, et al. Sequencing of neuroblastoma identifies chromothripsis and defects in neurogenesis genes. *Nature*. 2012; 483:589–593. [PubMed: 22367537]
12. Pugh TJ, et al. The genetic landscape of high-risk neuroblastoma. *Nat Genet*. 2013; 45:279–284. [PubMed: 23334666]
13. Sausen M, et al. Integrated genomic analyses identify ARID1A and ARID1B alterations in the childhood cancer neuroblastoma. *Nat Genet*. 2013; 45:12–17. [PubMed: 23202128]
14. Taggart D, Dubois S, Matthay KK. Radiolabeled metaiodobenzylguanidine for imaging and therapy of neuroblastoma. *The quarterly journal of nuclear medicine and molecular imaging*. 2008; 52:403–418. [PubMed: 19088694]
15. Schleiermacher G, et al. Emergence of New ALK Mutations at Relapse of Neuroblastoma. *J Clin Oncol*. 2014; 32:2727–2734. [PubMed: 25071110]
16. Carter SL, et al. Absolute quantification of somatic DNA alterations in human cancer. *Nat Biotech*. 2012; 30:413–421.
17. Boca SM, Kinzler KW, Velculescu VE, Vogelstein B, Parmigiani G. Patient-oriented gene set analysis for cancer mutation data. *Genome Biol*. 2010; 11:R112–11. [PubMed: 21092299]
18. Futreal PA, et al. A census of human cancer genes. *Nat Rev Cancer*. 2004; 4:177–183. [PubMed: 14993899]
19. Bresler S, et al. ALK Mutations Confer Differential Oncogenic Activation and Sensitivity to ALK Inhibition Therapy in Neuroblastoma. *Cancer Cell*. 2014; 26:682–694. [PubMed: 25517749]
20. Holzel M, et al. NF1 is a tumor suppressor in neuroblastoma that determines retinoic acid response and disease outcome. *Cell*. 2010; 142:218–229. [PubMed: 20655465]
21. Tartaglia M, et al. Diversity and functional consequences of germline and somatic PTPN11 mutations in human disease. *Am J Hum Genet*. 2006; 78:279–290. [PubMed: 16358218]
22. Carr-Wilkinson J, et al. High Frequency of p53/MDM2/p14ARF Pathway Abnormalities in Relapsed Neuroblastoma. *Clin Cancer Res*. 2010; 16:1108–1118. [PubMed: 20145180]
23. Garnett MJ, et al. Systematic identification of genomic markers of drug sensitivity in cancer cells. *Nature*. 2012; 483:570–575. [PubMed: 22460902]
24. Schleiermacher G, et al. Accumulation of Segmental Alterations Determines Progression in Neuroblastoma. *Journal of Clinical Oncology*. 2010; 28:3122–3130. [PubMed: 20516441]
25. Landau DA, et al. Evolution and impact of subclonal mutations in chronic lymphocytic leukemia. *Cell*. 2013; 152:714–726. [PubMed: 23415222]
26. Long GV. Increased MAPK reactivation in early resistance to dabrafenib/trametinib combination therapy of BRAF-mutant metastatic melanoma. *Nature Commun*. 2014; 5:5694. [PubMed: 25452114]
27. George RE, et al. Activating mutations in ALK provide a therapeutic target in neuroblastoma. *Nature*. 2008; 455:975–978. [PubMed: 18923525]
28. Mosse YP, et al. Safety and activity of crizotinib for paediatric patients with refractory solid tumours or anaplastic large-cell lymphoma: a Children's Oncology Group phase 1 consortium study. *Lancet Oncol*. 2013; 14:472–480. [PubMed: 23598171]
29. Berry T, et al. The ALKF1174L Mutation Potentiates the Oncogenic Activity of MYCN in Neuroblastoma. *Cancer Cell*. 22:117–130. [PubMed: 22789543]
30. Moore NF, et al. Molecular rationale for the use of PI3K/AKT/mTOR pathway inhibitors in combination with crizotinib in ALK -mutated neuroblastoma. *Oncotarget*. 2014; 5(18)
31. Drmanac R, et al. Human Genome Sequencing Using Unchained Base Reads on Self-Assembling DNA Nanoarrays. *Science*. 2010; 327:78–81. [PubMed: 19892942]
32. Favero F, et al. Sequenza: allele-specific copy number and mutation profiles from tumor sequencing data. *Annals of Oncology*. 2014
33. Krzywinski M, et al. Circos: An information aesthetic for comparative genomics. *Genome Research*. 2009; 19:1639–1645. [PubMed: 19541911]
34. Li H, Durbin R. Fast and accurate short read alignment with Burrows-Wheeler transform. *Bioinformatics*. 2009; 25:1754–1760. [PubMed: 19451168]
35. McKenna A, et al. The Genome Analysis Toolkit: A MapReduce framework for analyzing next-generation DNA sequencing data. *Genome Research*. 2010; 20:1297–1303. [PubMed: 20644199]

36. Cibulskis K, et al. Sensitive detection of somatic point mutations in impure and heterogeneous cancer samples. *Nat Biotech.* 2013; 31:213–219.
37. Wang K, Li M, Hakonarson H. ANNOVAR: functional annotation of genetic variants from high-throughput sequencing data. *Nucleic Acids Research.* 2010; 38:e164. [PubMed: 20601685]
38. An integrated map of genetic variation from 1, 092 human genomes. *Nature.* 2012; 491:56–65. [PubMed: 23128226]
39. Rausch T, et al. DELLY: structural variant discovery by integrated paired-end and split-read analysis. *Bioinformatics.* 2012; 28:i333–i339. [PubMed: 22962449]
40. Carter SL, et al. Absolute quantification of somatic DNA alterations in human cancer. *Nat Biotech.* 2012; 30:413–421.
41. Roth A, et al. PyClone: statistical inference of clonal population structure in cancer. *Nat Meth.* 2014; 11:396–398.
42. Lamers F, et al. Targeted BIRC5 silencing using YM155 causes cell death in neuroblastoma cells with low ABCB1 expression. *Eur J Cancer.* 2012; 48:763–771. [PubMed: 22088485]
43. Gnirke A, et al. Solution hybrid selection with ultra-long oligonucleotides for massively parallel targeted sequencing. *Nat Biotech.* 2009; 27:182–189.

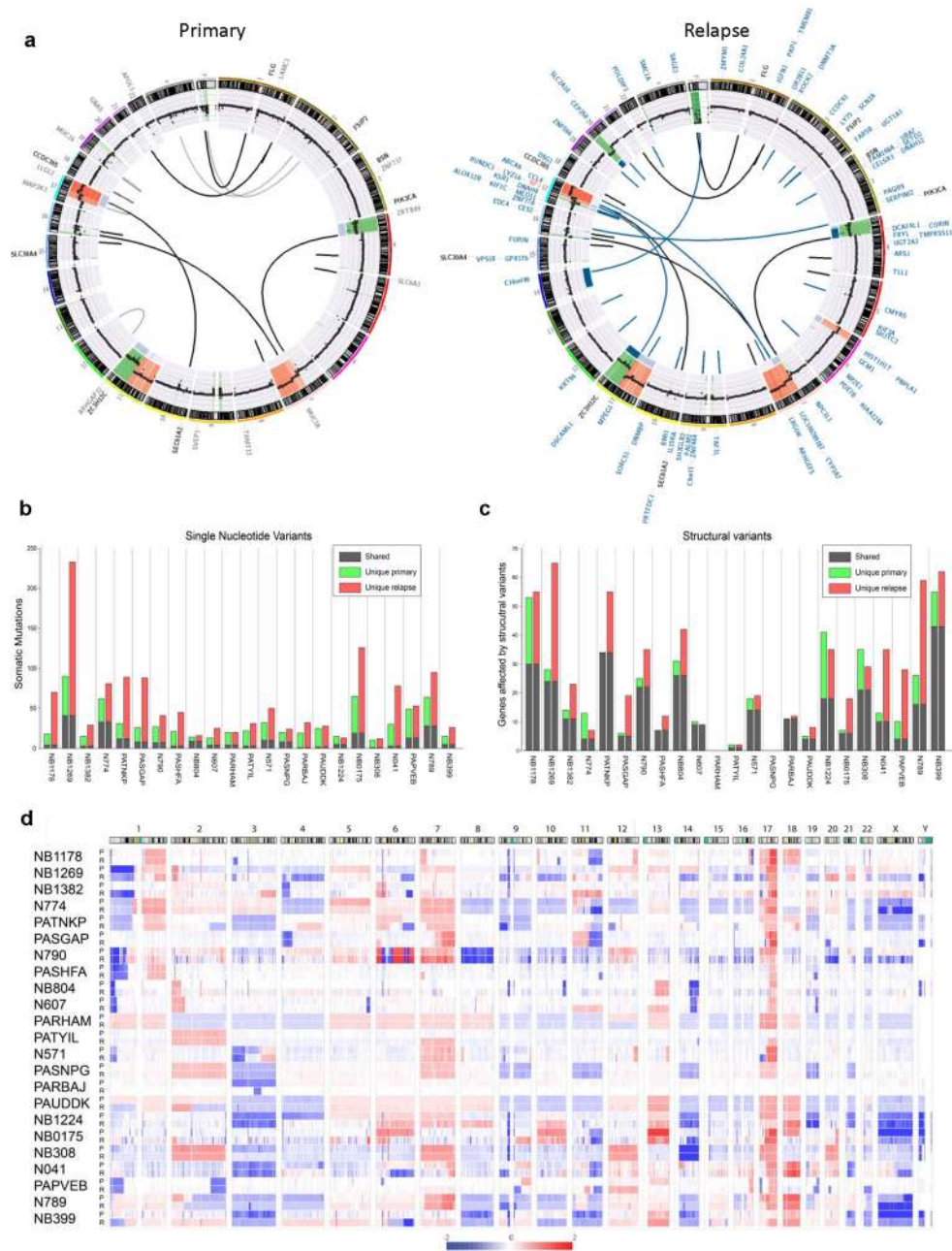


**Figure 1. Mutational spectrum of diagnostic and relapsed neuroblastomas**

**a)** Circos plots showing structural variations and somatic mutations in primary and corresponding relapse tumor of PASGAP. The inner ring represents the copy number variations (red, gain; green, loss) based on coverage of the tumor and lymphocyte genomes. The lines traversing the ring indicate inter- and intra-chromosomal rearrangements identified by discordant mate pairs from paired-end reads. Aberrations are colored based on their presence (grey = only detected in primary, black = detected in primary and relapse, blue = only detected in relapse, red = events predicted to activate RAS-MAPK signaling). **b)** The number of nonsynonymous mutations identified by WGS in 23 primary tumors and their

corresponding relapses. Mutations identified in both tumors are shown in grey while mutations unique for the primary or relapse tumor are shown in respectively green and red. **c)** The number of structural variants identified by WGS in 23 primary tumors and their corresponding relapses using same color scheme as panel b above. **d)** Coverage plots displaying the structural variations in primary and relapse tumors. Coverage was calculated for 1 Mb bins along the genome and normalized to the coverage in patient lymphocyte DNA. Color intensity reflects the magnitude of the gains or losses (blue=loss, red=gain) in the associated chromosomal location. P = primary; R = relapse

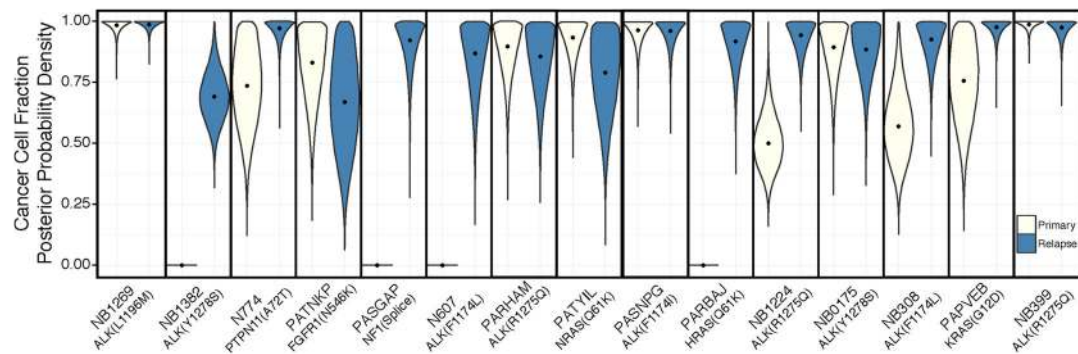


**Figure 2. RAS-MAPK pathway mutations reside within major relapsed neuroblastoma subclones**

Each of the 15 panels represents a primary-relapse pair with a corresponding RAS-MAPK pathway mutation. Posterior distributions of cancer cell fractions were computed by the method of Carter and colleagues<sup>16</sup> and are represented by violin plots with black dots drawn at the distribution medians. Four primary-relapse pairs (NB1382, PASGAP, N607, and PARBAJ) possess relapse-specific RAS-MAPK pathway mutations that are undetectable in the primary tumor by WGS. Three additional pairs (NB1224, NB308, and PAPVEB) also show evidence of relapse-specific enrichment of RAS-MAPK mutations based on a criterion of  $P(\text{CCFr} > \text{CCFp}) > 90\%$  for each pair. CCF estimates for ALK mutations in NB308 reflect F1174L(C>A) and F1174L(C>G) mutations in primary and relapse samples, respectively, as previously described<sup>15</sup>.

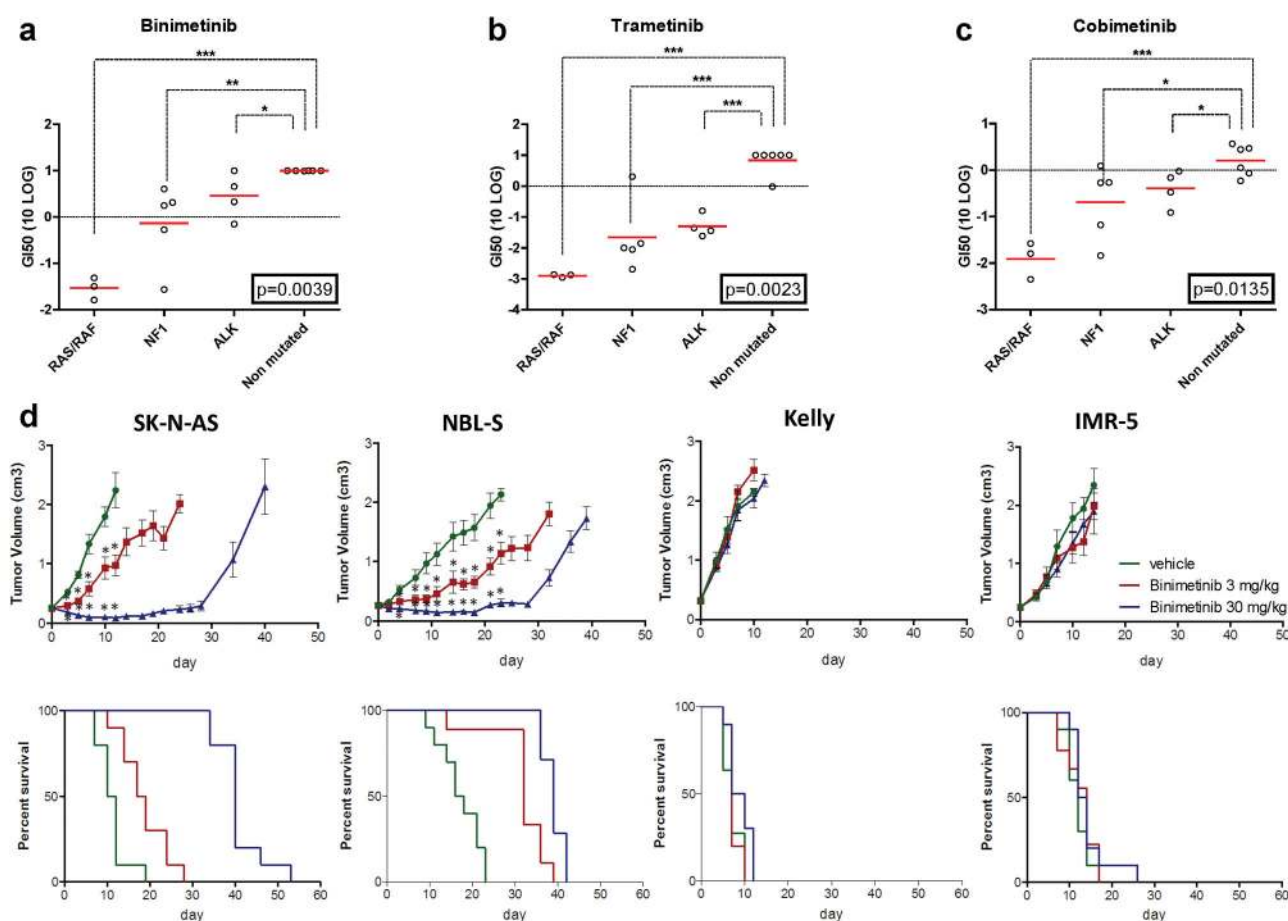


**Figure 3. Sensitivity of neuroblastoma cell lines models to MEK inhibition therapy**  
GI50 values for a panel of neuroblastoma cell lines treated with **a**) Binimetinib **b**) Trametinib and **c**) Cobimetinib. Cell lines are grouped according to their mutation status (Supplementary Table 6). P-values were derived from Kruskal-Wallis test. Student *t* test were performed to determine differences between non-mutated and mutated groups (\* =  $p<0.05$ , \*\* =  $p<0.01$ , \*\*\* =  $p<0.001$ ) **d**) Human neuroblastoma-derived SK-N-AS, NBL-S, Kelly and IMR-5 xenografts were treated with Binimetinib (3 mg/kg or 30 mg/kg) or vehicle by oral gavage twice daily. Each cohort consisted of ten mice, and tumor volumes (cm<sup>3</sup>) and percent survival are shown. Error bars represent standard error values and significance is denoted (\* =  $p<0.05$ ).

Table 1

Clinical characteristics of patient cohort.

Nr	Pat ID	Risk stratification	Stage	MYCN status	Gender	Age at diagnosis Months	Time to relapse Months after diagnosis	Time to last report Months after diagnosis	Status	Treatment (between diagnosis and relapse)			Diagnosis	Relapse
		INRG	INSS			Months	Months after diagnosis	Months after diagnosis		Radiation therapy	Chemo-therapy	Surgery	Location	Location
1	FR_NB1178	High	4	Non Amplified	M	30	21	24	Dead	Y	Y	Y	Retroperitoneum	Liver
2	FR_NB1269	High	4	Amplified	M	14	9	11	Dead	N	Y	Y	Retroperitoneum	Retroperitoneum
3	FR_NB1382	High	4	Amplified	M	4	50	64	Dead	N	Y	Y	Abdomen	Abdomen
4	NL_N774	High	4	Non Amplified	F	83	6	10	Dead	Y	Y	Y	Adrenal gland	Abdomen
5	US_PATNKP	High	4	Non Amplified	M	113	20	40	Alive	Y	Y	Y	Retroperitoneum	Pelvis
6	US_PASGAP	High	4	Non Amplified	M	44	42	51	Dead	Y	Y	Y	Adrenal gland	Soft tissue, skull
7	NL_N790	High	3	Amplified	F	42	63	110	Dead	Y	Y	Y	Adrenal gland	Liver
8	US_PASHFA	High	3	Amplified	F	13	7	11	Dead	N	Y	Y (Biopsy only)	Adrenal gland	Abdomen
9	FR_NB804	Intermediate	4	Non Amplified	F	2	26	56	Alive	N	Y	Y	Subcutaneous nodule	Orbita
10	NL_N607	Intermediate	4	Non Amplified	F	3	7	84	Alive	Y	Y	N	Liver	Orbita
11	US_PARHAM	Intermediate	4	Non Amplified	F	11	1	81	Dead	N	Y	N	Pelvis	Pelvis
12	US_PATYIL	Intermediate	4	Non Amplified	F	11	8	16	Dead	N	Y	Y	Abdomen	Pararenal
13	NL_N571	Intermediate	3	Non Amplified	M	49	12	16	Dead	N	Y	Y	Adrenal gland	Abdomen
14	US_PASNPG	Intermediate	3	Non Amplified	F	10	10	63	Alive	N	Y	Y	Retroperitoneum	Paraspinal
15	US_PARBAJ	Intermediate	3	Non Amplified	M	1	10	88	Alive	N	Y	Y	Retroperitoneum	Abdomen
16	US_PAUDDK	Intermediate	3	Non Amplified	M	12	11	38	Alive	N	Y	Y (Biopsy only)	Pelvis	Pelvis
17	FR_NB1224	Low	2	Non Amplified	M	15	8	18	Alive	N	Y	N	Mediastinum	Mediastinum
18	FR_NB0175	Low	2	Non Amplified	M	98	90	103	Dead	N	N	Y	Retroperitoneum	Retroperitoneum
19	FR_NB308	Low	2	Non Amplified	F	2	21	91	Alive	N	Y	N	Abdomen	Abdomen
20	NL_N041	Low	2	Non Amplified	F	109	72	92	Dead	Y	Y	Y	Abdomen	Abdomen
21	US_PAPVEB	Low	2	Non Amplified	M	57	9	40	Dead	N	N	N	Adrenal gland	Bone marrow
22	NL_N789	Low	1	Non Amplified	F	124	78	168	Alive	Y	Y	Y	Adrenal gland	Lymph node
23	FR_NB399	Low	4s	Non Amplified	M	0	7	134	Dead	N	Y	N	Subcutaneous nodule	Liver

**Table 2**

RAS-MAPK pathway mutations in relapsed neuroblastomas.

Nr	Pat ID	Genomic aberrations RAS-MAPK pathway in relapse tumors				Detected in primary tumor*
		Gene	genomic event	Type event	Cosmic ID	
1	FR_NB1178					
2	FR_NB1269	ALK	Somatic mutation (L1196M)	activating	99137	Yes
3	FR_NB1382	ALK	Somatic mutation (Y1278S)	activating	28058	No
4	NL_N774	PTPN11	Somatic mutation (A72T)	activating	13014	Yes
5	US_PATNKP	FGFR1	Somatic mutation (N546K)	activating	19176	Yes
6	US_PASGAP	NF1	Somatic Mutation (Splice Donor) + Hemizygous Deletion	inactivating		No
7	NL_N790	ALK	Amplification and fusion	activating		No
8	US_PASHFA					
9	FR_NB804					
10	NL_N607	ALK	Somatic mutation (F1174L)	activating	28055	No
11	US_PARHAM	ALK	Somatic mutation (R1275Q)	activating	28056	Yes
12	US_PATYIL	NRAS	Somatic mutation (Q61K)	activating	580	Yes
13	NL_N571	NF1	Homozygous deletion	inactivating		No
14	US_PASNPG	ALK	Somatic mutation (F1174L)	activating	28491	Yes
15	US_PARBAJ	HRAS	Somatic mutation (Q61K)	activating	496	No
16	US_PAUDDK					
17	FR_NB1224	ALK	Somatic mutation (R1275Q)	activating	28056	Yes
18	FR_NB0175	ALK	Somatic mutation (Y1278S)	activating	28058	Yes
19	FR_NB308	ALK	Somatic mutation (F1174L)	activating	28061	Yes
20	NL_N041	BRAF	Tandem duplication catalytic domain	activating		No
21	US_PAPVEB	KRAS	Somatic mutation (G12D)	activating	521	Yes
22	NL_N789					
23	FR_NB399	ALK	Somatic mutation (R1275Q)	activating	28056	Yes

\* based on WGS analysis